Hybrid Brain–Computer Interface for Controlling a Wearable Lower Limb Exoskeleton With Augmented Reality Glasses for Gait Assistance

Jinuk Kwon, Hyojeong Han, *Graduate Student Member, IEEE*, Jihun Hwang, Seungkyu Nam, Taejun Lee, Ho-Seung Cha, Kuk-Hyun Ahn, and Chang-Hwan Im

***Abstract*— Conventional crutch-based control for lower-limb exoskeletons often imposes a considerable physical burden and limits usability. To address these challenges, we developed a hybrid brain–computer interface (BCI) combining a steady-state visual evoked potential (SSVEP)-based BCI with asynchronous biosignal-based switches triggered by a wink and teeth clench. Practical usability was improved by implementing a wearable headband-type biosignal-recording device to acquire electroencephalography, electromyography, and electrooculography signals. Augmented reality glasses were used to present visual stimuli and gait guidance information. To support robust exoskeleton control in a wearable BCI environment, we proposed an asynchronous operational framework in which SSVEP responses were used for movement-mode selection, whereas wink- and clench-based switches were assigned to command execution and cancellation, respectively. Ten participants completed real-time walking experiments while wearing a custom lower-limb exoskeleton using both the conventional crutch-based and proposed control methods. The performance of the proposed system was evaluated using BCI classification accuracy and F1-scores for two asynchronous switches, whereas usability and workload were assessed using the system usability scale (SUS) and NASA task load index (NASA-TLX), respectively. Despite gross body movement during exoskeleton-assisted walking, the proposed hybrid control framework demonstrated robust mode selection, execution, and cancellation with an average SSVEP classification accuracy of 95.06%, F1-scores of 99.80% and 99.22% for the wink- and clench-based switches, respectively. Notably, only two false positive events were observed per switch across all participants. Furthermore, the proposed method exhibited a significantly higher SUS score than the crutch-based control method (78.25 vs. 53.50; $p < 0.01$) and a significantly lower physical demand in the NASA-TLX (3.15 vs. 7.85; $p < 0.05$), confirming its potential as a practical alternative. To the best of our knowledge, this is among the first studies in which a wearable hybrid SSVEP-based BCI for lower-limb exoskeleton operation applicable to real-world walking tasks was systematically demonstrated. Our findings suggest that the proposed hybrid BCI is a robust and less physically demanding alternative to a conventional control method, offering strong potential for daily assistance and gait rehabilitation.**

***Index Terms*— Brain–computer interface (BCI), steady-state visual evoked potential (SSVEP), hybrid BCI, lower-limb exoskeleton.**

Received 29 May 2026; revised 6 August 2026; accepted 29 August 2026. Date of publication 1 September 2026; date of current version 10 September 2026. Associate Editor: Imran Khan Niazi. This work was supported by Hyundai Motor Group. The work of Chang-Hwan Im was supported in part by the Artificial Intelligence Graduate School Program of Hanyang University funded by the Institute of Information and Communications Technology Planning and Evaluation (IITP) under Grant RS-2020-II201373. *(Jinuk Kwon and Hyojeong Han are co-first authors.) (Corresponding author: Chang-Hwan Im.)*

This work involved human subjects or animals in its research. Approval of all ethical and experimental procedures and protocols was granted by the Institutional Review Board (IRB) of Hanyang University, Republic of Korea under Application No. HYI-14-167-19.

Jinuk Kwon, Hyojeong Han, and Jihun Hwang are with the Department of Electronic Engineering, Hanyang University, Seoul 04763, Republic of Korea.

Seungkyu Nam, Taejun Lee, Ho-Seung Cha, and Kuk-Hyun Ahn are with the Robotics Laboratory, Research and Development Division, Hyundai Motor Company, Uiwang 16082, Republic of Korea.

Chang-Hwan Im is with the Department of Electronic Engineering and the Department of Biomedical Engineering, Hanyang University, Seoul 04763, Republic of Korea (e-mail: ich@hanyang.ac.kr).

Digital Object Identifier 10.1109/TNSRE.2026.3729803

I. Introduction

HUMAN mobility is a fundamental prerequisite for independent living; it enables individuals to perform daily activities and interact with their physical environment. However, this capability is often compromised by aging or chronic motor impairments, including stroke, spinal cord injury, Parkinson's disease, and other neuromuscular or musculoskeletal conditions, leading to a substantial reduction in the quality of life [1], [2]. Accordingly, wearable lower-limb exoskeletons have been developed as assistive technologies to augment locomotion and support user mobility in everyday environments [3]. With recent advances in robotics, these systems have increasingly transitioned to portable and wearable platforms suitable for complex real-world environments [4].

Despite these developments, powered wearable lower-limb exoskeletons typically rely on hand-operated control interfaces

© 2026 The Authors. This work is licensed under a Creative Commons Attribution-NonCommercial-NoDerivatives 4.0 License.
For more information, see https://creativecommons.org/licenses/by-nc-nd/4.0/

for gait initiation and mode switching, such as button-based remote controllers, smartphone applications, or joysticks [5], [6], [7]. Although such interfaces offer simplicity and reliability, they require continuous hand involvement, constraining the use of the upper limb, and imposing additional cognitive and physical demands on users. This limitation is particularly exacerbated in crutch-assisted configurations, where the user's upper limbs must be fully engaged in maintaining lateral stability and balance [8], [9]. Furthermore, the limited form factor of such interfaces inherently restricts the number and flexibility of available control commands. Consequently, the development of hands-free control strategies for alleviating users' physical burden and enabling more intuitive and seamless human–exoskeleton interactions has been attracting increasing attention [10], [11].

Recently, brain–computer interfaces (BCIs) have attracted considerable attention as a promising hands-free control modality for assistive and wearable robotic systems, enabling the direct inference of user intention from neural activity. Various neuroimaging modalities, including electrocorticography [12], electroencephalography (EEG) [13], magnetoencephalography [14], and functional near-infrared spectroscopy [15], have been used to measure neural activity in BCIs. Among these, EEG is the most widely adopted approach owing to its noninvasiveness, portability, relatively low cost, and high temporal resolution [16]. Two representative paradigms have been employed for decoding user intentions from EEG signals to induce discriminative neural activity patterns: (1) endogenous and (2) exogenous paradigms, depending on whether external stimuli are presented to the BCI users.

Endogenous paradigms rely on neural activity generated during intrinsic mental tasks, including motor imagery (MI) and inner speech, and offer an intuitive and self-paced control interface [17], [18]. Several studies have demonstrated the feasibility of MI-based BCIs for controlling lower-limb exoskeletons by decoding imagined lower-limb movements from EEG signals, with efforts to improve their performance and usability underway [19], [20], [21]. However, endogenous BCIs still face challenges related to robustness, training burden, and generalization across users and sessions owing to the inherent nonstationarity and low signal-to-noise ratio of EEG signals. Furthermore, the sustained mental effort required for MI tasks can increase the cognitive load and readily induce user fatigue, limiting their practical applicability in real-time settings [22], [23].

In contrast, exogenous BCIs rely on external periodic stimuli to elicit stimulus-locked neural responses, commonly referred to as steady-state evoked potentials, which are characterized by increased spectral power at the fundamental frequency of the stimulus and its harmonics [24], [25], [26]. Among them, steady-state visual evoked potentials (SSVEPs) are the most widely employed owing to their high performance, efficiency, and robustness in BCI-based exoskeleton control [27], [28]. Previous studies have demonstrated the control of powered lower-limb exoskeletons using SSVEP-based BCIs with high recognition accuracy, highlighting their reliability for gait-related control tasks [7], [29]. Moreover, researchers have recently attempted to improve the practicality and performance of SSVEP-based BCIs by introducing new interaction interfaces, such as augmented reality (AR) displays, and by developing advanced decoding algorithms, including deep-learning techniques and hybrid BCI strategies that combine complementary tasks or modalities [30], [31], [32], [33].

Despite substantial progress, several limitations hinder the application of BCI-controlled exoskeletons in real-world scenarios. First, in most previous studies, cap-based EEG systems with wired wet-type electrodes were utilized to ensure high decoding accuracy and reliability; this remains a major barrier because of the tedious and time-consuming setup process [22], [25]. Moreover, most experimental validations have been performed in laboratory settings or through simulations rather than in real-time experiments where users physically wear and operate exoskeletons during functional movements [4], [32], [33]. Thus, whether the existing BCI-based control strategies can be reliably translated into practical mobility-assistive or rehabilitation applications remains unclear. In addition, the robustness of the EEG-based control against motion-related artifacts that inevitably occur during actual exoskeleton operations remains unverified. Therefore, real-time experimental validation is essential to confirm whether BCI-based control strategies can maintain a reliable performance under such dynamic conditions.

In this study, we validated a fully wearable SSVEP-based hybrid BCI framework that combined EEG, electromyography (EMG), and electrooculography (EOG) signals to control a crutch-assisted lower-limb exoskeleton. A customized wireless headband-style wearable device equipped with eight dry electrodes was employed to record EEG signals from the occipital region, and two skin-attachable electrodes were used to record vertical EOG signals. Two asynchronous switches were implemented using EMG and EOG signals, which were triggered by a teeth clench and a wink, respectively. A lightweight glass-type portable AR device was employed to present SSVEP visual stimuli to enhance the real-world usability of the hybrid BCI system. Furthermore, visual guidance for crutch placement corresponding to upcoming movement commands was provided to improve user safety and operational convenience during the crutch-assisted operation of the lower-limb exoskeleton. The proposed system was evaluated through real-time experiments in which participants wore and operated a lower-limb exoskeleton while walking along predefined trajectories. It is to be noted that the lower-limb exoskeleton used in this study, developed by Hyundai Motor Company (Seoul, Republic of Korea), originally employed a conventional crutch-based button interface for control. Ten participants completed online experiments using both the crutch-button-based and proposed hybrid-BCI-based control approaches. The performance of the proposed system was evaluated in terms of the classification accuracy of the SSVEP-based BCI and the detection performance of EMG- and EOG-based asynchronous switches. Furthermore, the usability and task load of both control methods were assessed using a system usability scale (SUS) [34] and the NASA task load index (NASA-TLX) [35], respectively, to investigate the

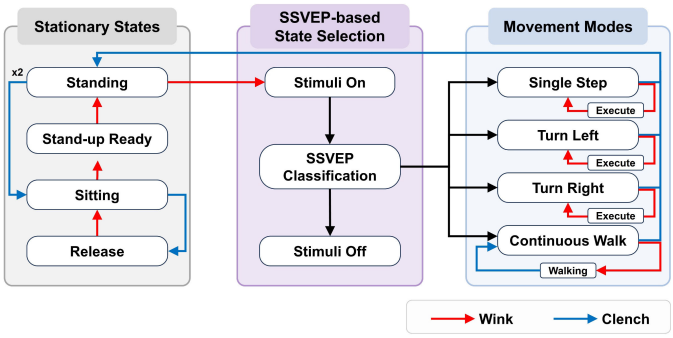


Fig. 1. Operational flowchart of the proposed BCI system. SSVEP is used for movement-mode selection, while wink and clench signals are used for command execution and movement-mode cancellation, respectively.

potential benefits of the hybrid-BCI-based operation of a real-world lower-limb exoskeleton.

The main contributions of this study are as follows: (1) development of a fully wearable hybrid BCI-based lower-limb exoskeleton control system integrating lightweight AR glasses and a wearable EEG device for practical locomotion assistance; (2) implementation of an asynchronous operational framework combining SSVEP-based movement-mode selection with wink- and clench-based command execution/cancellation, enabling stable operation under gross body movements during exoskeleton-assisted walking; (3) design of an AR-assisted user interaction framework providing real-time gait guidance and adaptive crutch-placement cues for intuitive exoskeleton operation; and (4) comprehensive experimental validation of the proposed hybrid BCI system during actual exoskeleton-assisted locomotion, including comparison with a conventional crutch-mounted remote-control method in terms of usability and physical workload.

II. Methods

A. Participants

Eleven healthy individuals (10 males and 1 female, aged 26.9 $\pm$ 3.42 years) volunteered in this study. However, one male participant was excluded from the practice sessions because he was unable to reliably execute the required wink task. Consequently, 10 participants (9 males and 1 female, aged 27.1 $\pm$ 3.53 years) completed the main online experiment. All the participants had normal or corrected-to-normal vision, and none reported a serious history of neurological, psychiatric, or other severe diseases that could have influenced the results. The study protocol was approved by the Institutional Review Board (IRB) of Hanyang University, Republic of Korea (IRB No. HYI-14-167-19) in accordance with the Declaration of Helsinki. Written informed consent was obtained from all the participants after a detailed explanation of the experimental procedures.

B. System Configuration

The overall configuration of the proposed hybrid BCI system is illustrated in Fig. 1. Figure 1(a) shows a snapshot of a user wearing the crutch-assisted lower-limb exoskeleton, and Figure 1(b) shows a system diagram depicting the roles of each device and their interconnections.

The exoskeleton (X-ble MEX; Hyundai Motor Company, Seoul, Republic of Korea) was customized by Hyundai Motor Company for comprehensive system control, enabling both crutch-based and hybrid-BCI-based operations. Detailed specifications of the X-ble MEX system are available on its official website: (https://robotics.hyundai.com/unveiled-robots/wearable/hmex.do). A commercial lightweight AR device, Nreal Air (Matrix Reality Technology Co. Ltd., China), was used to present the SSVEP stimuli and visual guidance, including the current state, required actions for state transitions, and crutch placement guides. A laptop computer (Surface Pro; Microsoft Corporation, USA) was mounted on the X-ble Mex and served as the central processing hub for communicating with the wearable EEG device, AR computing unit, and exoskeleton. The mounted computer was connected to the exoskeleton through serial communication and wirelessly received EEG/EOG signals from the EEG device via Bluetooth. Moreover, it exchanged exoskeleton status and stimulus control signals with the AR computing unit through TCP/IP communication.

An operational flowchart of the proposed system is presented in Fig. 2. The system supports four movement modes: single step, left turn, right turn, and continuous walk. Movement-mode selection was performed using SSVEP classification, whereas movement execution and cancellation were controlled using intentional wink and clench gestures, respectively. Within the current movement mode, an intentional wink executed the corresponding movement, whereas an intentional clench terminated the current movement mode and returned to the standing state. In the continuous-walk mode, once a wink was detected, the exoskeleton walked continuously until a clench was detected. In the continuous-walk mode, once a wink was detected, the exoskeleton walked continuously until a clench was detected. To ensure user safety and stability, the exoskeleton completed the current movement cycle before stopping, rather than halting immediately upon detecting a clenching command. Two consecutive clench actions were required to transition to a sitting state.

C. Data Recording

A customized wearable EEG headband was developed by modifying a commercial EEG device (MINDD SCAN; Ybrain, Seongnam, Republic of Korea), in collaboration with the original manufacturer, to specifically target the occipital region. Eight dry electrodes were arranged at O1, Oz, O2, PO7, PO3, POz, PO4, and PO8 according to the International 10-20 system. Flexible spiked-type electrodes were used to ensure stable scalp contact and robust signal quality. Two disposable adhesive electrodes were used to record the EOG signals, and the ground and reference electrodes were placed anterior and posterior to one earlobe, respectively. Signals were acquired at a sampling rate of 500 Hz. A 125 Hz signal was supplied during the device setup to assess the signal quality and turned off during the main experiments.

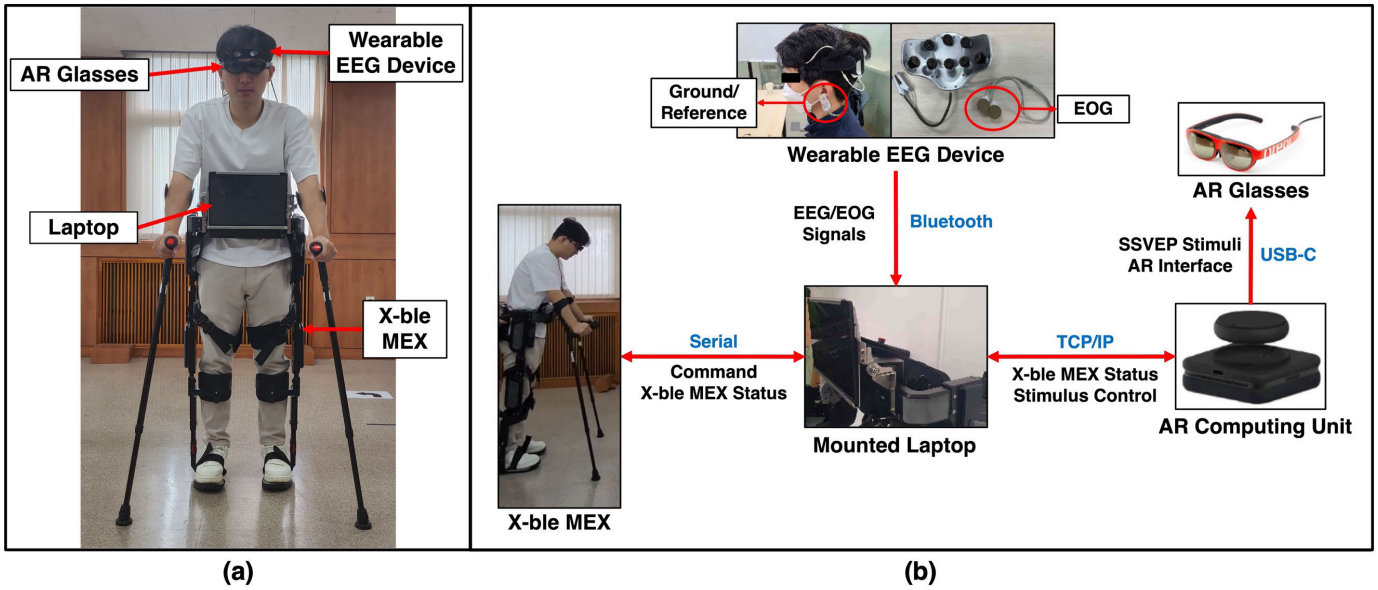


Fig. 2. Overall configuration and device interconnections of the proposed BCI-controlled exoskeleton system. (a) Example of a participant wearing the entire system. (b) System composition of the proposed hybrid-BCI-controlled exoskeleton.

D. Experimental Paradigms

Before the experiments, all the participants performed 10 SSVEP trials to assess potential SSVEP illiteracy [36]. Furthermore, the signals acquired during the wink and clench actions were visually inspected to confirm correct wink and clench executions. One participant was excluded because a single eye wink could not be reliably performed.

For safety reasons, practice sessions were conducted to familiarize the participants with the control methods for the crutch-assisted exoskeleton. While wearing the exoskeleton robot, the participants practiced both the conventional crutch-based and proposed BCI-based control methods until they became sufficiently accustomed to the system.

The main experiment consisted of two experimental sessions: conventional crutch-based control and proposed hybrid-BCI-based control. The session order was randomized across the participants to minimize potential learning effects, and the two sessions were performed on separate days. The predefined path for the experiments is illustrated in Fig. 3. Each experiment began at the starting point, indicated by the blue-colored area, where the participant was seated on a chair. After standing up, the participants moved along a predefined path using the single-step mode until they reached the black lines, where they were required to change their walking direction. In the orange areas, a continuous-walking mode was used to move to the next destination. Upon reaching the blue areas, the participants were instructed to sit down, either rest at the resting point or terminate the experiment at the endpoint. The entire task consisted of two standing actions, two sitting actions, and 20 SSVEP trials for walking mode selection, including eight single steps, two continuous walks, five left turns, and five right turns.

The timing sequence for the walking-mode selection and execution is illustrated in Fig. 4. Once a wink was detected

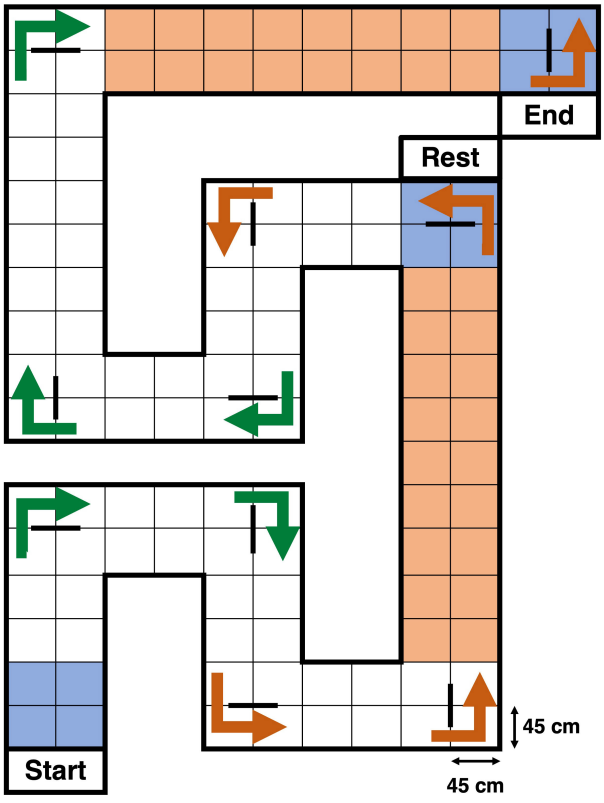


Fig. 3. Predefined experimental path. The blue-colored regions indicate the start, rest, and end areas, while the white and orange regions denote the single-step and continuous-walking sections, respectively. The bold black lines indicate the designated stopping points, and the arrows indicate the intended turning direction after each stop.

while the exoskeleton was in the standing state, a preparation period of 3 s was initiated, followed by the presentation of visual stimuli for 3 s. The SSVEP visual stimuli were

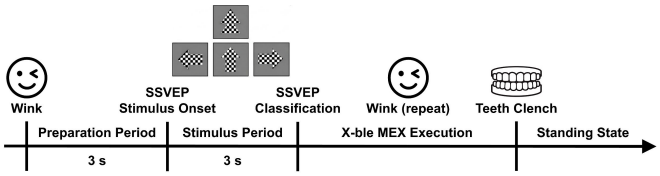


Fig. 4. Timing sequence of movement mode selection and execution.

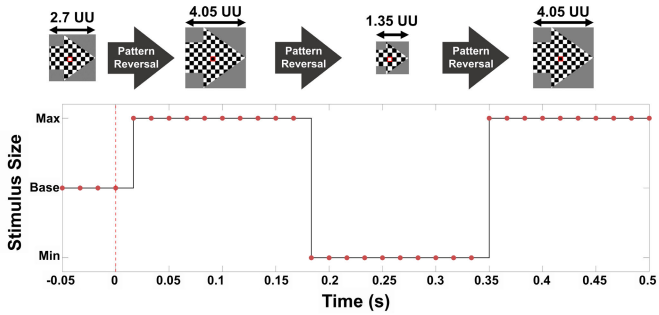


Fig. 5. PRS-based visual stimulus with square-wave periodic motion at 6 Hz. The red circles indicate the stimulus states presented at each frame according to the refresh rate of 60 Hz of the AR glasses. UU denotes the base unit used in Unity.

presented through the optical see-through AR glasses only during the movement-mode selection stage, allowing participants to simultaneously observe the surrounding real-world environment. The preparation period allowed the participants to prepare to gaze at a desired command. After classification, the current state information was displayed through the AR glasses. If the classification results matched the intended walking mode, a wink was used to execute the movement. Otherwise, a clench was used to return to the standing state, and the mode-selection procedure was repeated.

Upon the completion of each experiment, the participants evaluated the usability and workload of each control method using the Korean versions of the SUS and NASA-TLX, respectively.

E. Visual Stimuli for SSVEP

Based on our previous study [37], we employed a hybrid visual stimulus that combined pattern-reversal stimuli with square-wave periodic motion. Periodic motion was implemented by varying the stimulus size by 50%, whereas the size of the individual checkerboard grids remained unchanged. The temporal modulation sequence of the 6 Hz visual stimulus is illustrated in Fig. 5.

Three arrow-shaped stimuli corresponding to "single step," "turn left," and "turn right" flickered at 6 (= 60/10), 6.67 (= 60/9), and 7.5 (= 60/8) Hz, respectively. For "continuous walking", a double-triangle-shaped stimulus flickering at 10 (= 60/6) Hz was used. A gray background was presented behind each visual stimulus to enhance visibility. The stimulation frequencies were selected considering the refresh rate (60 Hz) of the AR glasses and determined using integer divisions to ensure precise and stable stimulus presentation.

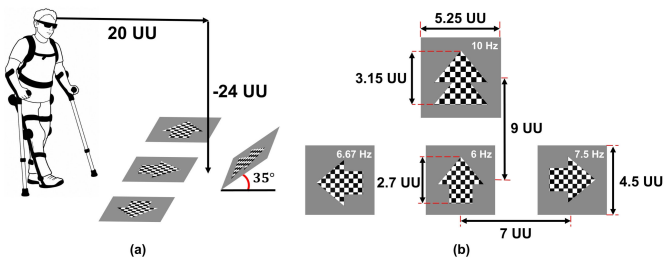


Fig. 6. (a) Configuration of the visual stimuli designed in the Unity environment. (b) Size and spatial arrangement of the four SSVEP visual stimuli. UU denotes the Unity base unit.

The visual stimuli were designed using the Unity engine (Unity 2022.3.62f3; Unity Technologies ApS, USA). Detailed settings, including the stimulus size, interstimulus spacing, and stimulus locations relative to the Unity camera, are shown in Fig. 6. All the spatial dimensions are represented in units used in Unity (UU). The stimulus size and spatial locations were determined from preliminary experiments to balance SSVEP performance, visual fatigue, and usability in the AR environment. Specifically, the stimulus was selected to maximize SSVEP performance while avoiding excessive visual fatigue, whereas the spatial locations were arranged to minimize unnecessary head movements while maintaining comfortable visual discrimination among stimuli.

F. AR-Based User Interface

The AR interface was designed to provide users with the real-time system status and the required actions for state transitions during the exoskeleton operation. The current state of the exoskeleton was displayed at the center of the AR interface. The next state triggered by the winking action was presented on the right side, whereas the state transition caused by the clench action was displayed on the left side. A circular marker was presented above the current state information to indicate whether the exoskeleton was in motion or stationary, represented by red and green, respectively. No additional commands were accepted while the circular marker was displayed in red.

In addition to the AR interface for user convenience, an AR-based crutch placement guide was developed to facilitate rapid adaptation for novice users. Transparent light green circles were overlaid on the floor to indicate the optimal crutch positions. When the exoskeleton was moving, the next optimal crutch position was displayed more opaquely to emphasize the upcoming placement location. By visualizing the crutch placement required for a stable gait through the AR display, the system reduced the time required for users to become familiar with the equipment and ensured postural stability during the initial training phase.

An example of the single-step mode is displayed in Fig. 7. When the single-step mode was selected, the right foot was highlighted in the current state panel. The movement to be executed after a wink input was displayed on the right side, allowing the user to recognize which foot would move next. The left-hand panel displayed the standing state that would be

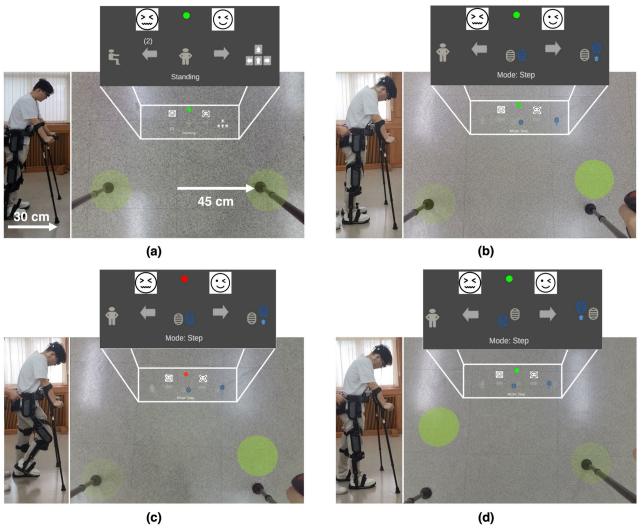


Fig. 7. Example of the AR-based interface and crutch placement guide during single-step mode. (a) Standing state, (b) single-step mode, (c) single-step execution in progress, and (d) completion of single-step movement.

transitioned to after a clench action. In this case, the trailing foot moved forward while returning to the standing state. Demonstration videos of the AR user interface are available at https://youtu.be/tpm6FCu0COM?si=v1_pIw4LSY19-I1q.

G. Signal Processing

All signal processing, including SSVEP classification and wink and clench detection, was implemented using MATLAB (MathWorks, Inc., USA). Filtering was performed using sixth-order zero-phase Butterworth filters. All classification and detection procedures were implemented using training-free algorithms. Therefore, no model training, training/testing split, or cross-validation procedure was involved in the evaluation.

1) **SSVEP Classification** After the visual stimuli ended, the raw EEG signals were segmented into the most recent interval of 5 s, consisting of a classification window of 3 s and an additional margin of 2 s to alleviate filtering distortion. The segmented EEG signals were bandpass filtered with the cutoff frequencies of 2 and 54 Hz to eliminate low-frequency baseline drift and power line noise. Subsequently, the latest 2.865 s of the filtered signals were used, after excluding the margin of 2 s and compensating for a visual pathway latency of 0.135 s [38].
Subharmonic filter bank canonical correlation analysis (sFBCCA) [37], an extension of the standard filter bank canonical correlation analysis (FBCCA) [39], was employed for SSVEP classification. The sFBCCA also incorporates subharmonic components induced by the periodic motion of the hybrid visual stimuli. For the fundamental and harmonic components, all the parameters followed the original FBCCA configuration. A filter bank with five subbands was used, with the cutoff frequency ranges of 4–52, 8–52, 12–52, 16–52, and 20–52 Hz. For the subharmonic component, the same parameters used for the second harmonic were applied, and a bandpass filter with the cutoff frequencies of 1 and 52 Hz was applied. The reference signal includes fundamental, harmonic, and subharmonic frequencies.
2) **Wink Detection** A speed-threshold-based method [40] was adapted and modified to detect intentional winking signals. Gaussian smoothing with a 100-sample window was applied to each EOG channel to suppress noise, followed by a baseline correction relative to the first sample to eliminate the baseline drift. The differential signal between the left and right channels ($EOG_{diff} = EOG_L - EOG_R$) was utilized to maximize the ocular asymmetry occurring during a unilateral wink.
Although the conventional speed-threshold-based method typically employs three parameters—speed, amplitude, and duration—our preliminary tests demonstrated that the speed parameter alone provided sufficient detection accuracy. Consequently, the algorithm was modified to track the absolute value of the first-order derivative (f') of EOG_{diff} to monitor the rate of signal change over time, enabling the unified detection of both the left and right winks.
The multicondition inspection scheme proposed by Ma et al. [40] was adopted to simultaneously examine three consecutive slopes (f'_t, f'_{t+1}, and f'_{t+2}) to precisely determine the onset and offset of each wink using the following equations:

$$tl_1 = \left\{t \middle| |f'_t| < S \wedge |f'_{t+1}| \geq S \wedge |f'_{t+2}| \geq S\right\}; \quad (1)$$

$$tl_2 = \left\{t \middle| |f'_t| \geq S \wedge |f'_{t+1}| \geq S \wedge |f'_{t+2}| < S\right\}. \quad (2)$$

Here, tl_1 and tl_2 denote the onset and offset candidates for rapid signal changes based on the predefined speed threshold S, respectively. The identified interval is defined as a valid wink segment after verifying the temporal order of the detected indices. Within this segment, the peak-to-peak amplitudes of the left and right EOG channels were compared to determine wink direction. The speed threshold (S) was empirically set to 2.5 from preliminary experiments.
3) **Clench Detection** For clench detection, a root mean square (RMS)-based algorithm was implemented to identify simultaneous high-amplitude EMG artifacts across the EEG and EOG signals. The most recent data segment of 0.5 s was bandpass filtered with the frequency range of 150–245 Hz. A clench event was detected when the RMS values of all eight EEG channels and two EOG channels simultaneously exceeded the empirically determined thresholds of 4 and 5, respectively.

III. Results

A. SSVEP Classification Accuracy

Table I summarizes the SSVEP classification accuracy across the participants using a window of 3 s, used during real-time operation. The average classification accuracy is 95.06 ± 4.85% (mean ± standard deviation). Nine out of 10 participants achieve accuracies higher than 90%, with more

TABLE I
SSVEP CLASSIFICATION ACCURACY ACROSS PARTICIPANTS USING A WINDOW OF 3 S

Participant	P1	P2	P3	P4	P5	P6	P7	P8	P9	P10	Mean ± SD
Total Trials	23	21	20	21	21	20	23	22	22	20	21.30 ± 1.16
Correct Trials	20	20	20	21	20	20	21	20	20	20	20.20 ± 0.42
Accuracy (%)	86.96	95.24	100.00	100.00	95.24	100.00	91.30	90.91	90.91	100.00	95.06 ± 4.85

SD: standard deviation

TABLE II
WINK DETECTION PERFORMANCES

Participant	Side	FN	FP	Recall (%)	Precision (%)	F1-Score (%)
P1	L	0	0	100.00	100.00	100.00
P2	L	0	1	100.00	99.33	99.66
P3	R	0	1	100.00	99.34	99.67
P4	L	0	0	100.00	100.00	100.00
P5	R	3	0	98.08	100.00	99.03
P6	R	0	0	100.00	100.00	100.00
P7	R	0	0	100.00	100.00	100.00
P8	R	0	0	100.00	100.00	100.00
P9	L	0	0	100.00	100.00	100.00
P10	L	0	1	100.00	99.29	99.64
Mean ± SD		0.30 ± 0.95	0.30 ± 0.48	99.81 ± 0.61	99.80 ± 0.33	99.80 ± 0.32

FN: false negative, FP: false positive, SD: standard deviation

TABLE III
CLENCH DETECTION PERFORMANCES

Participant	FN	FP	Recall (%)	Precision (%)	F1-Score (%)
P1	0	0	100.00	100.00	100.00
P2	0	1	100.00	96.43	98.18
P3	1	0	96.15	100.00	98.04
P4	0	1	100.00	96.15	98.04
P5	1	0	96.00	100.00	97.96
P6	0	0	100.00	100.00	100.00
P7	0	0	100.00	100.00	100.00
P8	0	0	100.00	100.00	100.00
P9	0	0	100.00	100.00	100.00
P10	0	0	100.00	100.00	100.00
Mean ± SD	0.20 ± 0.42	0.20 ± 0.42	99.22 ± 1.65	99.26 ± 1.57	99.22 ± 1.01

FN: false negative, FP: false positive, SD: standard deviation

than half of the participants (six) achieving a classification accuracy of 100%. The average number of trials per participant was 21 ± 1.16, exceeding the 20 trials required to complete the predefined task under ideal conditions because additional movement-mode selections were occasionally required following SSVEP misclassifications.

B. Asynchronous Switches

The performances of the proposed asynchronous switches are summarized in Tables II and III for wink- and clench-based switches, respectively. The performance is evaluated using recall, precision, and F1-score as evaluation metrics.

1) **Wink Detection** For wink detection, the average recall, precision, and F1-score across the participants are 99.81 ± 0.61%, 99.80 ± 0.33%, and 99.80 ± 0.32% (mean ± standard deviation), respectively, indicating high sensitivity in capturing user intentions while maintaining strong robustness against unintended signals or noise. In particular, most participants achieve near-perfect recall (100.0% for 9 out of 10 participants), whereas the precision is higher than 99.0% for all the participants. These results demonstrate that the proposed wink-based asynchronous switch can reliably detect user commands with excellent performance, even during lower-limb exoskeleton operations. The high F1-score further confirms a well-balanced tradeoff between sensitivity and precision. Notably, the preference for the winking side is balanced between the left and right sides across the participants, suggesting no side-specific performance bias.
2) **Clench Detection** For clench detection, the average recall, precision, and F1-score are 99.22 ± 1.65%, 99.26 ± 1.57%, and 99.22 ± 1.01% (mean ± standard deviation), respectively, also demonstrating reliable detection performance during lower-limb exoskeleton operation.

Only a few errors are observed, with two participants showing one false negative (FN) each, and two participants showing one false positive (FP) each. These results indicate that the clench-based asynchronous switch

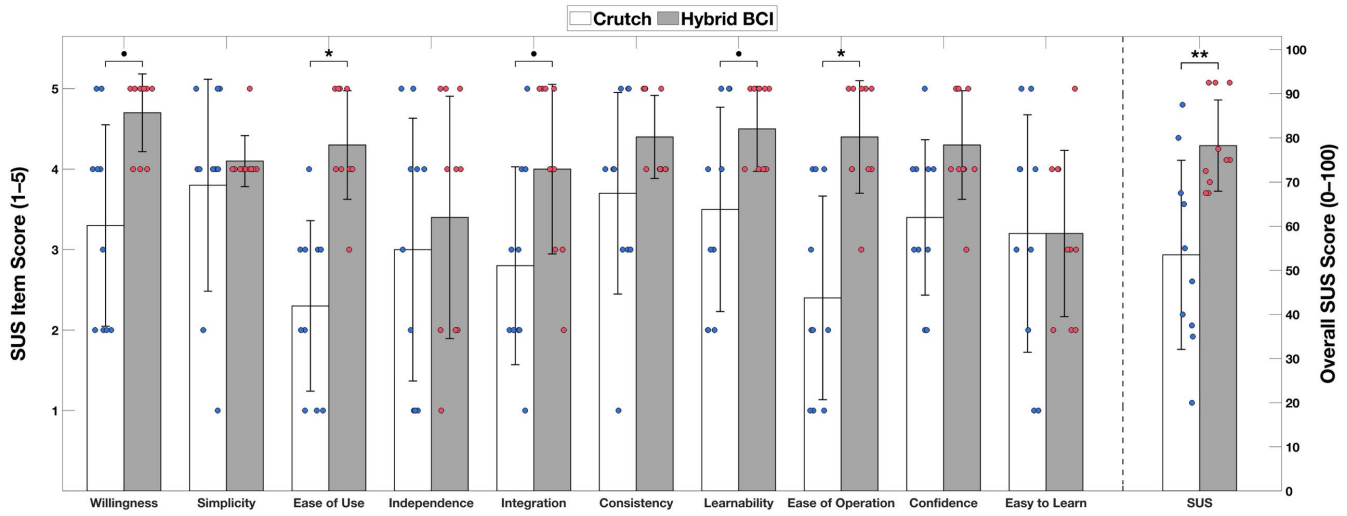


Fig. 8. Average responses to individual SUS items and overall SUS scores for the crutch-based (white) and hybrid BCI-based (gray) control methods. Dots represent individual participants' responses, and error bars represent standard deviations across participants. Negatively worded items were reverse-scored so that higher scores indicate better usability. $\bullet p < 0.1$, $^{*}p < 0.05$, and $p < 0.01^{**}$ indicate a statistical significance between the two methods (Wilcoxon signed-rank test). FDR correction was applied to the comparisons of the 10 individual SUS items.

provides stable and responsive control signals for hybrid BCI systems under dynamic walking conditions.

Overall, both asynchronous switches achieve near-perfect detection performance even without participant-specific optimization during noisy real-time operations.

The operational flow of the proposed hybrid BCI system, including the AR interface, real-time exoskeleton control for each gait mode, and full experimental procedure, is presented in https://youtu.be/tpm6FCu0COM?si=v1_pIw4LSY19-I1q.

C. Survey

1) **System Usability**
Figure 8 presents a comparison of the average responses to the individual SUS items and the overall SUS scores for the crutch-based (white bars) and proposed hybrid-BCI-based (gray bars) control interfaces across the participants. Each dot represents the response of an individual participant, and the error bars denote the standard deviations. Negatively worded SUS items are reverse-scored such that higher scores consistently indicate more favorable usability. The scores for the willingness to use, simplicity, ease of use, independence, well-integrated functions, consistency, learnability, ease of operation, confidence, and low learning burden are presented for both control methods in the left panel of the figure. Notably, the scores for ease of use and ease of operation show statistically significant differences, whereas the scores for willingness to use, well-integrated functions, and learnability show marginal significance ($^{*}p < 0.05$, $p < 0.1$, Wilcoxon signed-rank test, FDR corrected). The average SUS scores are 53.50 ± 21.42 and 78.25 ± 10.34 for the crutch- and hybrid-BCI-based control methods, respectively. All the participants report higher overall usability for the proposed hybrid-BCI-based interface than for the conventional crutch-based control. Statistical analysis conducted using the Wilcoxon signed-rank test reveals a significant difference between the two control methods ($p < 0.01$).

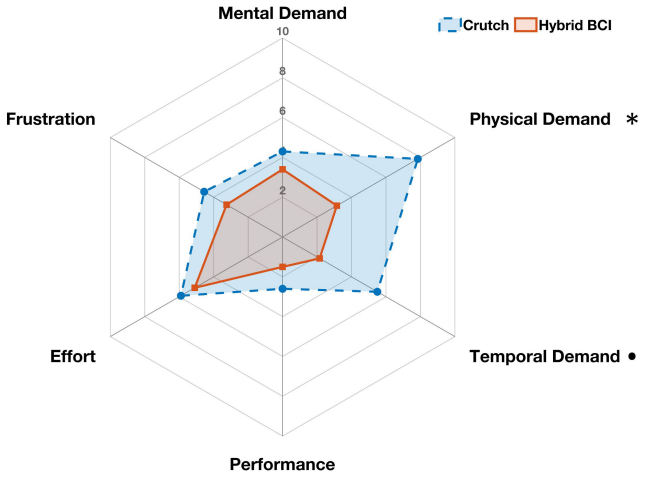


Fig. 9. Subjective workload assessment using the NASA-TLX. Comparison between crutch- and hybrid-BCI-based control methods across six dimensions. Lower scores indicate lower perceived workload, except for performance, where lower scores represent higher perceived success. The asterisks (*) and circles ($\bullet$) indicate statistical significance at $p < 0.05$ and $p < 0.10$, respectively (Wilcoxon signed-rank test with FDR correction).

1) **Workload** Figure 9 illustrates the subjective workload evaluated using the NASA-TLX. For crutch-based control, the average scores are 4.30 ± 3.52, 7.85 ± 2.85, 5.50 ± 3.17, 2.60 ± 2.44, 5.90 ± 2.83, and 4.55 ± 3.80 (mean $\pm$ standard deviation) for mental demand, physical demand, temporal demand, performance, effort, and frustration, respectively. The average scores for mental demand, physical demand, temporal demand, performance, effort, and frustration for the

proposed hybrid-BCI-based control are 3.40 ± 2.44, 3.15 ± 2.51, 2.15 ± 1.89, 1.50 ± 1.08, 5.10 ± 2.26, and 3.25 ± 2.63, respectively. Lower scores indicate a lower perceived workload, whereas lower scores in the performance dimension denote better task success. Physical demand exhibits a significantly lower score for the hybrid-BCI-based control ($p < 0.05$, Wilcoxon signed-rank test with FDR correction). Moreover, the temporal demand shows a marginally significant reduction ($p < 0.10$). Although not statistically significant, the other dimensions show lower scores in the hybrid BCI condition, suggesting an improved user experience.

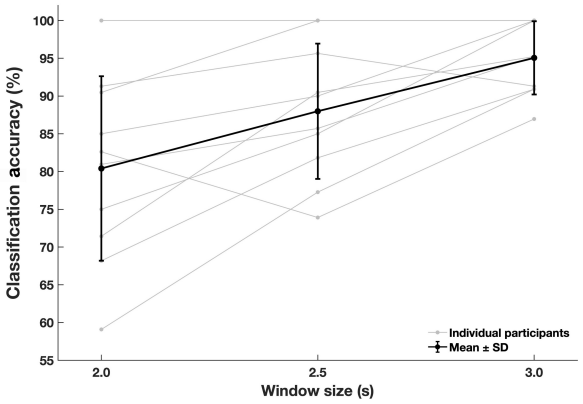


Fig. 10. Classification accuracy as a function of the window size. The gray lines indicate individual participants, whereas the black line denotes the mean and standard deviation across participants. The mean classification accuracies are 80.40 ± 12.22%, 87.98 ± 8.96%, and 95.06 ± 4.85% for the window sizes of 2.0, 2.5, and 3.0 s, respectively.

IV. Discussion

In this study, we investigated the feasibility of an SSVEP-based hybrid BCI for controlling a crutch-assisted lower-limb exoskeleton, with the aim of improving usability and reducing the physical burden associated with conventional crutch-based control. The proposed system was implemented as an asynchronous control framework to enable robust exoskeleton operation in a wearable BCI environment. Within this framework, an SSVEP-based BCI was used for movement-mode selection, while wink- and clench-based biosignal switches were employed for command execution and cancellation, respectively. This design enabled users to select, execute, and cancel exoskeleton control commands without relying on hand-operated interfaces during walking. The experimental results demonstrated that the proposed hybrid BCI framework could reliably support real-time exoskeleton control during actual walking. Importantly, the system maintained high classification and detection performance despite motion artifacts and muscle activity inherent to crutch-assisted locomotion, conditions that have rarely been considered in previous evaluations of BCI reliability. The achieved SSVEP classification accuracy of 95.06%, together with F1-scores of 99.80% and 99.22% for the wink- and clench-based switches, respectively, further confirms the robustness of the proposed control architecture for real-time operation under movement-related noise encountered during walking.

Furthermore, the SUS and NASA-TLX scores showed that the proposed hybrid-BCI-based control provided significantly higher usability and lower physical demand than conventional crutch-based control methods. Although the usability was evaluated by healthy participants, the average SUS score was 78.25, which was considerably higher than the minimum acceptance level of 70. Moreover, the proposed system showed a lower overall workload than conventional crutch-based control, suggesting its promising potential as an alternative control interface for crutch-assisted lower-limb exoskeletons. To the best of our knowledge, this is the first study in which a hybrid SSVEP-based BCI control interface for crutch-assisted lower-limb exoskeleton operation is evaluated during actual user operation and its usability and workload are systematically compared with those of conventional crutch-based control.

The considerably higher usability and reduced workload observed in this study demonstrated the effectiveness of the proposed hybrid BCI system, which was further enhanced by the intuitive design of the integrated AR interface. Because a lightweight glass-type AR device was employed, the proposed system simplified one of the major limitations of conventional SSVEP-based BCIs, namely, the presentation of visual stimuli and user interaction during operation. Because the SSVEP stimuli, robotic status information, and visual feedback were integrated directly into the user's field of view, the system provided users with intuitive guidance regarding the current system status, upcoming actions, and required user commands. This integration minimized the need to shift attention between the surrounding environment and the external control screen, thereby enabling a more convenient and intuitive interaction during exoskeleton-assisted locomotion. Furthermore, the operational stability of the hybrid BCI was supported by AR-based crutch placement guides, which provided essential spatial information for optimal crutch positioning to maintain balance and reduce physical strain. Although visual discomfort was not quantitatively assessed, no participants voluntarily reported noticeable discomfort or adaptation difficulties while using the AR glasses during the experimental sessions.

In this study, we achieved a high average classification accuracy of 95.06% using a window of 3 s with a wearable EEG system employing dry electrodes. The use of dry electrodes eliminates the need for gel application and additional hair washing, making the system more convenient for daily use. Although the results demonstrate the strong potential of the proposed interface, there remains room for further improvement in the decoding performance and overall practicality. The classification performance decreased rapidly when using a smaller window size. As shown in Fig. 10, the average classification accuracies for the window sizes of 2.0, 2.5, and 3.0 s are 80.40 ± 12.22%, 87.98 ± 8.96%, and 95.06 ± 4.85% (mean ± standard deviation), respectively. Compared with conventional control interfaces, a window of 3.0 s may still be relatively long for real-world applications that require more responsive control. Fortunately, several recent studies have demonstrated that advances in signal processing and deep-learning methods enable reliable SSVEP decoding with considerably shorter time windows. For example, a conven-

tional neural network-based approach achieved a classification accuracy of approximately 90% with a window of 0.5 s for four targets [41], and a transformer-based approach reported a comparable performance with a window of 1.1 s for 12 targets and a classification accuracy of 85% for 40 targets [42]. Considerable efforts have been devoted to improving the signal quality so that the performance becomes comparable to that of wet electrodes through advanced signal processing techniques [43], [44]. Therefore, future studies should investigate approaches to achieve high-performance SSVEP decoding with a shorter window size, further enhancing practicality. Another limitation of the current study is that the proposed system supports only a limited number of movement commands. Future studies should expand the command set to enable more flexible exoskeleton control in real-world environments. Furthermore, the proposed framework was evaluated only in a single-session experiment. Multi-session evaluations are needed to investigate long-term robustness, user adaptation, and sustained usability.

Our results reveal the robust performance of the proposed biosignal-based asynchronous switches during active exoskeleton operations. The participants could execute or stop commands using winking and teeth-clenching gestures while walking with a crutch-assisted lower-limb exoskeleton. The system exhibited a high detection performance despite the substantial body movements and strong muscle activities caused by crutch-assisted locomotion, which could potentially generate motion artifacts and degrade signal reliability. Moreover, for asynchronous switches, FPs are generally more critical than FNs because unintended activations may lead to unsafe or undesired system behaviors, whereas missed detections can typically be corrected by generating the command again. In this study, the proposed switches showed only a few FPs (one occurrence for three participants in winking and one occurrence for two participants in teeth clenching) while maintaining high recall and precision across the participants. Notably, all the parameters were identically applied to every participant without subject-specific optimization, and the system showed a consistently high performance. These results suggest that the proposed wink- and clench-based asynchronous switches exhibit promising robustness and generalizability for reliable exoskeleton control. Furthermore, incorporating simple subject-specific parameter tuning may further improve detection reliability and responsiveness, particularly for future patient studies.

Although our results demonstrated that the proposed hybrid-BCI-based control interface significantly reduced the physical demand compared with conventional crutch-based control, the experiments in this study were conducted only with healthy participants, who are not the main target users of lower-limb exoskeleton systems. The results obtained from healthy participants suggest that the potential benefits of the proposed system may be even more pronounced in patients who frequently experience substantial physical burdens when operating conventional control interfaces. As the control task in this study was physically demanding, even for healthy participants, patients with motor impairments may face even greater difficulty. In this regard, the proposed BCI-based control interface provides a more accessible and less physically demanding alternative for exoskeleton operations. Furthermore, the relatively low workload observed in this study (Fig. 9) suggests that the proposed system may have significant potential in rehabilitation settings where exoskeleton-assisted gait training is used to support functional recovery. Although the sample size was relatively limited, statistically significant differences between the two control methods were observed in both usability and workload evaluations, providing preliminary support for the feasibility of the proposed framework. Nevertheless, given the limited number of participants and the inclusion of only healthy individuals, the present findings should be interpreted primarily as evidence of feasibility rather than as validation of generalizability to the broader population or intended clinical users. Future studies should therefore evaluate the proposed system in a substantially larger cohort, particularly including patient populations who represent the intended end users of lower-limb exoskeleton systems. Such studies will be necessary to further establish the usability, effectiveness, generalizability, and potential clinical impact of the proposed framework.

REFERENCES

[1] G. Kwakkel and B. J. Kollen, "Predicting activities after stroke: What is clinically relevant?" *Int. J. Stroke*, vol. 8, no. 1, pp. 25–32, Jan. 2013.

[2] N. Butsing, J. G. Voss, J. Keandoungchun, N. Thongniran, and M. T. Q. Griffin, "Changes of health-related Quality of life within 6 months after stroke by clinical and sociodemographic factors," *Sci. Rep.*, vol. 15, no. 1, p. 416, Jan. 2025.

[3] A. M. Dollar and H. Herr, "Design of a quasi-passive knee exoskeleton to assist running," in *Proc. IEEE/RSJ Int. Conf. Intell. Robots Syst.*, Sep. 2008, pp. 747–754.

[4] L. Ferrero et al., "Brain–machine interface based on deep learning to control asynchronously a lower-limb robotic exoskeleton: A case-of-study," *J. NeuroEngineering Rehabil.*, vol. 21, no. 1, p. 48, Apr. 2024.

[5] K. A. Strausser and H. Kazerooni, "The development and testing of a human machine interface for a mobile medical exoskeleton," in *Proc. IEEE/RSJ Int. Conf. Intell. Robots Syst.*, Sep. 2011, pp. 4911–4916.

[6] G. Zeilig, H. Weingarden, M. Zwecker, I. Dudkiewicz, A. Bloch, and A. Esquenazi, "Safety and tolerance of the ReWalk exoskeleton suit for ambulation by people with complete spinal cord injury: A pilot study," *J. Spinal Cord Med.*, vol. 35, no. 2, pp. 96–101, Mar. 2012.

[7] Y. He, D. Eguren, J. M. Azorín, R. G. Grossman, T. P. Luu, and J. L. Contreras-Vidal, "Brain–machine interfaces for controlling lower-limb powered robotic systems," *J. Neural Eng.*, vol. 15, no. 2, Apr. 2018, Art. no. 021004.

[8] S. Federici, F. Meloni, M. Bracalenti, and M. L. De Filippis, "The effectiveness of powered, active lower limb exoskeletons in neurorehabilitation: A systematic review," *NeuroRehabilitation*, vol. 37, no. 3, pp. 321–340, Nov. 2015.

[9] D. R. Louie and J. J. Eng, "Powered robotic exoskeletons in post-stroke rehabilitation of gait: A scoping review," *J. NeuroEngineering Rehabil.*, vol. 13, no. 1, p. 53, Dec. 2016.

[10] D. Torricelli et al., "Benchmarking wearable robots: Challenges and recommendations from functional, user experience, and methodological perspectives," *Frontiers Robot. AI*, vol. 7, Nov. 2020, Art. no. 561774.

[11] Y.-P. Zhang, G.-Z. Cao, L.-L. Li, and D.-F. Diao, "Interactive control of lower limb exoskeleton robots: A review," *IEEE Sensors J.*, vol. 24, no. 5, pp. 5759–5784, Mar. 2024.

[12] G. Schalk et al., "Two-dimensional movement control using electrocorticographic signals in humans," *J. Neural Eng.*, vol. 5, no. 1, pp. 75–84, Mar. 2008.

[13] V. J. Lawhern, A. J. Solon, N. R. Waytowich, S. M. Gordon, C. P. Hung, and B. J. Lance, "EEGNet: A compact convolutional neural network for EEG-based brain–computer interfaces," *J. Neural Eng.*, vol. 15, no. 5, Oct. 2018, Art. no. 056013.

[14] S. Roy, D. Rathee, A. Chowdhury, K. McCreadie, and G. Prasad, "Assessing impact of channel selection on decoding of motor and cognitive imagery from MEG data," *J. Neural Eng.*, vol. 17, no. 5, Oct. 2020, Art. no. 056037.

[15] J. Kwon and C.-H. Im, "Subject-independent functional near-infrared spectroscopy-based brain–computer interfaces based on convolutional neural networks," *Frontiers Hum. Neurosci.*, vol. 15, Mar. 2021, Art. no. 646915.

[16] R. Abiri, S. Borhani, E. W. Sellers, Y. Jiang, and X. Zhao, "A comprehensive review of EEG-based brain–computer interface paradigms," *J. Neural Eng.*, vol. 16, no. 1, 2019, Art. no. 011001.

[17] C. Zhang, Y.-K. Kim, and A. Eskandarian, "EEG-inception: An accurate and robust end-to-end neural network for EEG-based motor imagery classification," *J. Neural Eng.*, vol. 18, no. 4, Aug. 2021, Art. no. 046014.

[18] N. Padfield, K. Camilleri, T. Camilleri, S. Fabri, and M. Bugeja, "A comprehensive review of endogenous EEG-based BCIs for dynamic device control," *Sensors*, vol. 22, no. 15, p. 5802, Aug. 2022.

[19] M. Tariq, P. M. Trivailo, and M. Simic, "EEG-based BCI control schemes for lower-limb assistive-robots," *Frontiers Hum. Neurosci.*, vol. 12, Aug. 2018, Art. no. 312.

[20] M. S. Al-Quraishi, I. Elamvazuthi, S. A. Daud, S. Parasuraman, and A. Borboni, "EEG-based control for upper and lower limb exoskeletons and prostheses: A systematic review," *Sensors*, vol. 18, no. 10, p. 3342, Oct. 2018.

[21] J. Choi, K. T. Kim, J. H. Jeong, L. Kim, S. J. Lee, and H. Kim, "Developing a motor imagery-based real-time asynchronous hybrid BCI controller for a lower-limb exoskeleton," *Sensors*, vol. 20, no. 24, p. 7309, Dec. 2020.

[22] F. Lotte et al., "A review of classification algorithms for EEG-based brain–computer interfaces: A 10 year update," *J. Neural Eng.*, vol. 15, no. 3, Jun. 2018, Art. no. 031005.

[23] A. Colucci et al., "Brain–computer interface-controlled exoskeletons in clinical neurorehabilitation: Ready or not?" *Neurorehabilitation Neural Repair*, vol. 36, no. 12, pp. 747–756, Dec. 2022.

[24] N. Kaongoen and S. Jo, "A novel hybrid auditory BCI paradigm combining ASSR and P300," *J. Neurosci. Methods*, vol. 279, pp. 44–51, Mar. 2017.

[25] R. Zerafa, T. Camilleri, O. Falzon, and K. P. Camilleri, "To train or not to train? A survey on training of feature extraction methods for SSVEP-based BCIs," *J. Neural Eng.*, vol. 15, no. 5, Oct. 2018, Art. no. 051001.

[26] J. Petit, J. Rouillard, and F. Cabestaing, "EEG-based brain–computer interfaces exploiting steady-state somatosensory-evoked potentials: A literature review," *J. Neural Eng.*, vol. 18, no. 5, Oct. 2021, Art. no. 051003.

[27] X. Xing et al., "A high-speed SSVEP-based BCI using dry EEG electrodes," *Sci. Rep.*, vol. 8, no. 1, p. 14708, Oct. 2018.

[28] Y. Chen, C. Yang, X. Ye, X. Chen, Y. Wang, and X. Gao, "Implementing a calibration-free SSVEP-based BCI system with 160 targets," *J. Neural Eng.*, vol. 18, no. 4, Aug. 2021, Art. no. 046094.

[29] N.-S. Kwak, K.-R. Müller, and S.-W. Lee, "A lower limb exoskeleton control system based on steady state visual evoked potentials," *J. Neural Eng.*, vol. 12, no. 5, Oct. 2015, Art. no. 056009.

[30] F. Wang, Y. Wen, J. Bi, H. Li, and J. Sun, "A portable SSVEP-BCI system for rehabilitation exoskeleton in augmented reality environment," *Biomed. Signal Process. Control*, vol. 83, May 2023, Art. no. 104664.

[31] Z. An, F. Wang, Y. Wen, F. Hu, and S. Han, "A real-time CNN-BiLSTM-based classifier for patient-centered AR-SSVEP active rehabilitation exoskeleton system," *Expert Syst. Appl.*, vol. 255, Dec. 2024, Art. no. 124706.

[32] L. Liu et al., "Multimodal brain-controlled system for rehabilitation training: Combining asynchronous Online brain–computer interface and exoskeleton," *J. Neurosci. Methods*, vol. 406, Jun. 2024, Art. no. 110132.

[33] Y. Wang and J. Yao, "AgileEEG: A lightweight CNN enabling real-time BCI control of a portable rehabilitation exoskeleton," *J. Supercomput.*, vol. 81, no. 16, p. 1537, Nov. 2025.

[34] J. R. Lewis, "The system usability scale: Past, present, and future," *Int. J. Hum.–Comput. Interact.*, vol. 34, no. 7, pp. 577–590, Jul. 2018.

[35] S. G. Hart, "NASA-task load index (NASA-TLX); 20 years later," in *Proc. Hum. Factors Ergonom. Soc. Annu. Meeting*, 2006, vol. 50, no. 9, pp. 904–908.

[36] B. Allison, T. Luth, D. Valbuena, A. Teymourian, I. Volosyak, and A. Graser, "BCI demographics: How many (and what kinds of) people can use an SSVEP BCI?" *IEEE Trans. Neural Syst. Rehabil. Eng.*, vol. 18, no. 2, pp. 107–116, Apr. 2010.

[37] J. Kwon, J. Hwang, H. Nam, and C.-H. Im, "Novel hybrid visual stimuli incorporating periodic motions into conventional flickering or pattern-reversal visual stimuli for steady-state visual evoked potential-based brain–computer interfaces," *Frontiers Neuroinform.*, vol. 16, Sep. 2022, Art. no. 997068.

[38] M. M. Müller, W. Teder-Sälejärvi, and S. A. Hillyard, "The time course of cortical facilitation during cued shifts of spatial attention," *Nature Neurosci.*, vol. 1, no. 7, pp. 631–634, Nov. 1998.

[39] X. Chen, Y. Wang, S. Gao, T.-P. Jung, and X. Gao, "Filter bank canonical correlation analysis for implementing a high-speed SSVEP-based brain–computer interface," *J. Neural Eng.*, vol. 12, no. 4, Aug. 2015, Art. no. 046008.

[40] J. Ma, Y. Zhang, A. Cichocki, and F. Matsuno, "A novel EOG/EEG hybrid human–machine interface adopting eye movements and ERPs: Application to robot control," *IEEE Trans. Biomed. Eng.*, vol. 62, no. 3, pp. 876–889, Mar. 2015.

[41] W. Ding, J. Shan, B. Fang, C. Wang, F. Sun, and X. Li, "Filter bank convolutional neural network for short time-window steady-state visual evoked potential classification," *IEEE Trans. Neural Syst. Rehabil. Eng.*, vol. 29, pp. 2615–2624, 2021.

[42] J. Chen, Y. Zhang, Y. Pan, P. Xu, and C. Guan, "A transformer-based deep neural network model for SSVEP classification," *Neural Netw.*, vol. 164, pp. 521–534, Jul. 2023.

[43] B. Liu, X. Chen, X. Li, Y. Wang, X. Gao, and S. Gao, "Align and pool for EEG headset domain adaptation (ALPHA) to facilitate dry electrode based SSVEP-BCI," *IEEE Trans. Biomed. Eng.*, vol. 69, no. 2, pp. 795–806, Feb. 2022.

[44] M. Zhang et al., "DECAN: A denoising encoder via contrastive alignment network for dry electrode EEG emotion recognition," 2024, *arXiv:2409.03976*.